Mon. Not. R. Astron. Soc. **310**, L27–L32 (1999)

High-redshift evolution of optical- and infrared-selected galaxies: a comparison with cold dark matter scenarios

Adriano Fontana,[1] Nicola Menci,[1] Sandro D'Odorico,[2] Emanuele Giallongo,[1] Francesco Poli,[1] Stefano Cristiani,[3,4] Alan Moorwood[2] and Paolo Saracco[5]

[1]*Osservatorio Astronomico di Roma, 00040 Monte Porzio, Italy*
[2]*European Southern Observatory, 85748 Garching bei München, Germany*
[3]*Dipartimento di Astronomia dell' Università, 35122 Padova, Italy*
[4]*Space Telescope European Coordinating Facility, European Southern Observatory, 85748 Garching bei München, Germany*
[5]*Osservatorio Astronomico di Brera, 22055 Merate (LC), Italy*

Accepted 1999 October 11. Received 1999 September 10; in original form 1999 July 30

ABSTRACT

A combination of ground-based (NTT and VLT) and *Hubble Space Telescope* (*HST*) (HDF–N and HDF–S) public imaging surveys has been used to collect a sample of 1712 *I*-selected and 319 $K \leq 21$ galaxies observed with an extended spectral coverage from *U* to *K* bands. Photometric redshifts have been obtained for all these galaxies, using a spectral library computed from Bruzual & Charlot models. The results have been compared with the prediction of an analytic rendition of the current cold dark matter (CDM) hierarchical models for galaxy formation that explicitly accounts for magnitude limits and dust extinction. We focus in particular on two observed quantities: the galaxy redshift distribution at $K \leq 21$ and the evolution of the UV luminosity density. The former has been proposed by Kauffmann & Charlot to be a very robust prediction of any CDM hierarchical model, and we show that it is remarkably constant among different cosmological models. The derived photometric redshift distribution is in agreement with the hierarchical CDM prediction, with a fraction of only 5 per cent of galaxies detected at $z \geq 2$. This result strongly supports hierarchical scenarios where present-day massive galaxies are the result of merging processes. The observed UV luminosity density in our *I*-selected sample is confined within a factor of 4 over the whole range $0 < z < 4.5$, in agreement with previous spectroscopic and photometric surveys. CDM models in a critical ($\Omega = 1$, $\Lambda = 0$) Universe are not able to produce the density of UV photons that is observed at $z \geq 3$. CDM models in a Λ-dominated universe are in better agreement at $3 \leq z \leq 4.5$, but predict a pronounced peak at $z \simeq 1.5$ and a drop by a factor of 8 from $z = 1.5$ to $z = 4$ that is not observed in the data. We conclude that improvements are required in the treatment of the physical processes directly related to the star formation rate (SFR), e.g. the starburst activity in merger processes and/or different recipes for linking the supernova feedback to the star formation activity.

Key words: galaxies: distances and redshifts – galaxies: evolution – cosmology: observations – cosmology: theory – infrared: galaxies.

1 INTRODUCTION

Understanding how massive galaxies formed and evolved is one of the major goals of present-day cosmology. Currently favoured theoretical scenarios attempt to describe ab initio the global formation and evolution of galaxies from primordial fluctuations, including the main physical processes involved (e.g. Kauffmann, White & Guiderdoni 1993; Cole et al. 1994; Baugh et al. 1998). These 'hierarchical' models naturally predict that galaxies form from smaller units that accrete gas and merge to build up present-day massive objects. These models are challenged by several observations, suggesting that bulges and ellipticals were formed at a very early stage of the Universe and slowly evolved thereafter (Bernardi et al. 1999; Schade et al. 1999 and references therein).

Kauffmann & Charlot (1998; KC98 hereafter) proposed the use of the redshift distribution of *K*-band limited samples to address this issue. The main advantage here is that the *K* band traces the IR radiation produced by ordinary stars at any $z \leq 4$ (see fig. 1 of KC98) and is little affected by dust extinction, and it is therefore a reliable tracer of the mass in stars already assembled in galaxies at

any redshift. As shown by KC98, hierarchical models prevent massive galaxies from being already assembled at $z \geq 1$, and the expected number of galaxies at $z \geq 1.5$ is about 4 times lower than the predictions of pure luminosity evolution (PLE) models. Unfortunately, the existing spectroscopic surveys (Cowie et al. 1996; Cohen et al. 1999) still lack the required completeness at faint IR magnitudes in this critical redshift regime.

The evolution of the global star formation rate (SFR) as a function of z has long been recognized a powerful tool to trace galaxy evolution. The first results from spectroscopic (Lilly et al. 1995) and colour-estimated (Madau et al. 1996; Madau, Pozetti & Dickinson 1998; Connolly et al. 1997) redshift surveys suggested a steep rise and fall of the SFR with a main peak at $z \simeq 2$. Photometric redshift analysis (Giallongo et al. 1998, hereafter G98; Pascarelle et al. 1998) and spectroscopic surveys at low and high z (Treyer et al. 1998; Cowie, Songaila & Barger 1999; Steidel et al. 1999), inclusion of dust corrections and far-IR detections (Hughes et al. 1998) are now modifying this picture.

In this work we have used deep ground-based and *Hubble Space Telescope* (*HST*) multiband observations from UV to IR to obtain photometric redshifts for galaxies in optical ($I < 27.5$) and IR ($K < 21$) samples. The redshift distributions of the K-band limited sample and the UV luminosity density have been compared with the results of cold dark matter (CDM) models to test their fundamental properties.

2 THE BASIC INGREDIENTS: DATA AND MODELS

2.1 Multicolour catalogues

The observations used in this paper cover the full wavelength range from UV to K bands and have subarcsec image quality. Two of the fields were observed with the ESO 3.5 New Technology Telescope (NTT) SUSI imager: the first (hereafter BR1202) is centred on the $z = 4.7$ QSOBR1202-07, the second is a neighbouring field (NTT Deep Field, NTTDF hereafter). The *BVRI* images and catalogues of these fields are described in G98 and Arnouts et al. (1999a) respectively, complemented by NTT observations in J and K (Saracco et al. 1999) and in the U band. The latter observations and the procedures to obtain the final *UBVRIJK* catalogues are fully described in Fontana et al. (in preparation).

The third data set results from the VLT-NICMOS observations of the HDF–S (Fontana et al. 1999).

Finally, we have used the HDF–N and HDF–S with the IR observations obtained at Kitt Peak and at NTT–SOFI (Da Costa et al. 1998), respectively. For the HDF–N we have used the multicolour catalogue published by Fernandez-Soto, Lanzetta & Yahil (1999), which uses an optimal technique to match the optical and IR images that have a quite different seeing. A similar catalogue for the HDF–S has been provided by the same authors and is available at the URL only http://www.ess.sunysb.edu/astro/hfds/home.html. Only WFPC bands have been used in the optical, for consistency with the HDF–N. In both cases we have clipped the outer regions of the frame with lower signal-to-noise ratio (S/N).

Despite different origins, these data are sufficiently homogeneous for the purpose of the paper. Indeed, all catalogues have been obtained with similar procedures and software, and we have obtained photometric redshifts only for objects that are largely above the detection threshold, so that small differences in the detection procedures are not expected to be important. All the multicolour catalogues use the optical images as detection frame, as this is appropriate for the estimate of the UV luminosity density at high redshift. We have also performed an independent object detection on the K images alone to ensure that all the galaxies at $K < 21$ were included in our optically selected catalogues.

2.2 Photometric redshifts

The multicolour catalogues have been used to derive photometric redshifts for all the galaxies in the sample, using a code already described elsewhere (G98; Fontana et al. in preparation). The code is based on the synthetic models of the Bruzual & Charlot GISSEL library, with the addition of intergalactic absorption (Madau et al. 1996) and dust reddening (Small Magellanc Cloud like: Pei 1992). The accuracy on the HDF–N spectroscopic sample is $\sigma_z \sim 0.06$ (0.3) in the redshift interval $z = 0$–1.5 (1.5–3.5).

At fainter flux levels the reliability of photometric redshift has been estimated with Monte Carlo simulations (Arnouts et al. 1999b). We have defined a bright sample at $I_{AB} \leq 26$ that includes a subsample of the two HDFs and the NTTDF, and a fainter HDF(N+S) sample to $I_{AB} \leq 27.5$.

It is known that Galactic stars are significant sources of false high redshift candidates, especially in the brightest samples (Steidel et al. 1999). Obvious stars have been excluded at $I_{AB} \leq 25.5$ in the HDF–S on the basis of the SEXTRACTOR morphological classification (Arnouts et al. 1999a). The morphological selection removes all the $z \geq 5$ candidates in the HDF–S. These objects are typically bright ($I = 20$–24) and are always detected in the *JHK* bands. They would be formally assigned to $z \geq 5$, because they are nearly undetected in V and have a negative $J - K$, typical of M star spectra. Analogously, we have used the detailed morphological classification developed in Poli et al. (1999) to identify stars down to $I_{AB} \simeq 25.3$ in the NTTDF sample.

2.3 An analytical rendition of hierarchical models

To compare these results with the present understanding of galaxy formation and evolution we have developed an analytical rendition of the hierarchical models (e.g. Cole et al. 1994). The prescription used to treat all the physical processes involved is identical to the 'Durham' rendition, and we refer the reader to Cole et al. (1994) and Baugh et al. (1998) for the details, while the complete formulations of our analytical rendition are given in Poli et al. 1999 (see also Menci & Cavaliere 1999). Rather than following the history of each halo within a Monte Carlo scheme, we produce the statistical distributions of the main physical properties of galaxies in the dark matter (DM) haloes. Our treatment extends the White & Frenk (1991) approach, explicitly including the merging of galaxies in common haloes through dynamical friction. This is accomplished by computing for all galaxies in DM haloes the probability that the dynamical friction time is smaller than the halo survival time (as given by Lacey & Cole 1993). For the average quantities of interest here, this approach produces the same outputs as the 'Durham' approach. We emphasize that we have not attempted to modify or improve the current models, which have several free parameters tuned to match the local properties of galaxies (counts, the I-band Tully–Fisher relation and the B-band luminosity function), because our aim is simply to compare the model predictions with the picture emerging from our data.

The only improvement introduced is a self-consistent treatment

of the dust absorption, by defining an effective optical depth τ_λ (Guiderdoni & Rocca-Volmerange 1987) that is used to suppress the expected luminosity:

$$\tau_\lambda = \tau^0_{\rm dust}(1-\omega)^{1/2}(A_\lambda/A_V)(Z_{\rm g}/Z_\odot)^s f_{\rm g}, \quad (1)$$

where $(1-\omega)^{1/2}(A_\lambda/A_V)(Z_{\rm g}/Z_\odot)^s$ is a metal-dependent extinction law, $f_{\rm g}$ is the gas fraction $f_{\rm g} = m_{\rm g}/(m_{\rm g}+m_*)$ (computed by the code) and $\tau^0_{\rm dust}$ is a gas-to-dust ratio chosen to match the observed B luminosity function at low redshift (Somerville & Primack 1998).

We adopt in this paper four different models: a standard CDM (SCDM: $\Omega = 1, \Lambda = 0, h = 0.5$), an open CDM ($\Omega = 0.5, \Lambda = 0, h = 0.7$), a low-density flat model (ΛCDM: $\Omega = 0.3, \Lambda = 0.7, h = 0.6$) and a tilted model, ($\Omega = 1$: $\Lambda = 0, h = 0.5$). The power-spectrum normalization and the parameters that describe the initial mass function (IMF), the star formation process and the galaxy merging are taken from Heyl et al. (1995) for SCDM, open and ΛCDM models, and from Poli et al. (1999) for the tilted model.

3 THE $K < 21$ SAMPLES

The normalized cumulative redshift distributions of the 319 objects in the K-limited sample are shown in Fig. 1. The upper panel shows the different distributions in the five fields considered here as well as the total distribution. The results from the five fields are clearly consistent, within the observed field-to-field scatter. As expected, the most discordant distributions come from the two smallest fields (BR1202 and VLTTC). For the purpose of the KC98 test, what is critical is the number of massive high-z galaxies detected in the sample. Only 9 per cent of the galaxies are found at $z \geq 1.6$ (8, 7 and 12 per cent in the NTTDF, HDF–N and HDF–S respectively); this becomes 5 per cent at $z \geq 2$ (6, 4 and 2 per cent). A similar conclusion was reached by Saracco et al. (1999).

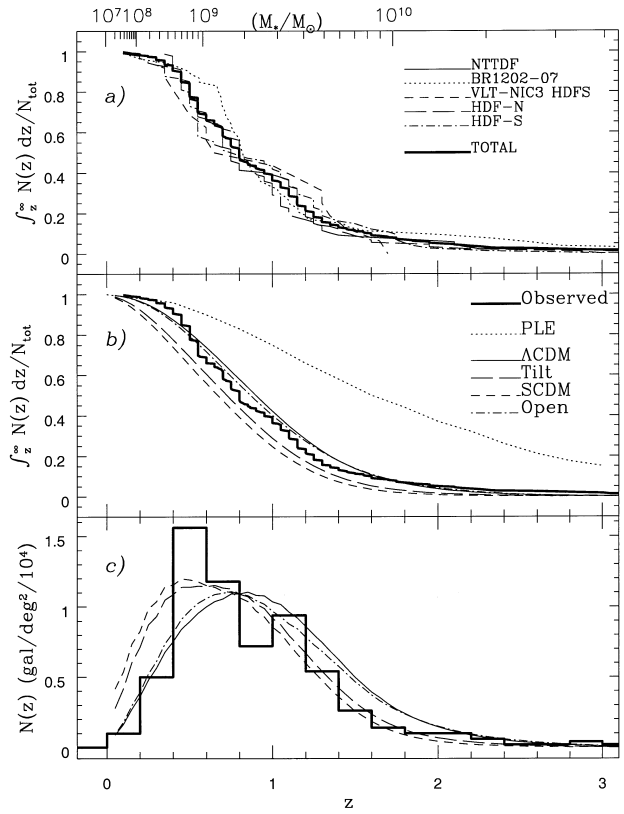

Figure 1. Redshift distribution at $K \leq 21$. (a) Observed normalized cumulative distribution of a total of 319 galaxies in five fields. Thin lines: individual distributions (see legend for details). Thick line: total distribution. (b) Comparison between the total cumulative distribution of the upper panel and theoretical predictions of the four CDM models described in the text and of the PLE model. (c) Comparison between the observed differential redshift distribution and the CDM predictions. The upper axis of panel (a) shows the mass in stars contained in an evolved galaxy at the corresponding redshift, normalized to $K = 21$. A Miller–Scalo IMF, age of 2 Gyr, solar metallicity and star formation time-scale of 0.1 Gyr were adopted.

In the middle panel, the total distribution is compared with the predictions of PLE models (as adopted from KC98) and the CDM models described in the previous section. All the CDM models are reasonably consistent with each other, despite the wide variety of cosmological and physical parameters adopted. As expected, the open and Λ models predict slower evolution. Conversely, there is a large difference between the ensemble of hierarchical models and the PLE predictions in the KC98 rendition. This fact, which was already stressed by KC98, applies not only to the SCDM used by KC98 but also to other models with different cosmologies, strengthening the validity of the KC98 test.

A main result of the paper is that *the observed cumulative distribution is in good agreement with that predicted by the hierarchical models*, strongly supporting hierarchical scenarios where massive objects are the result of merging processes in recent epochs.

To reiterate that the $K \leq 21$ threshold corresponds to a selection with respect to the mass of the galaxies, we have labelled the upper x-axis of Fig. 1 with the mass of stars contained in an evolved galaxy at the corresponding redshift, normalized to $K = 21$. At $z \geq 1.6$, the minimum mass in stars in objects at $K \leq 21$ is $\simeq 10^{10}\,{\rm M}_\odot$. However, a significant contribution to the K luminosity may also result from the asymptotic giant branch (AGB) population during a starburst phase. For comparison, the same $K = 21$ luminosity may be obtained from a $z = 1.6$ galaxy of only 0.1 Gyr age with a constant star formation rate of $10\,{\rm M}_\odot\,{\rm yr}^{-1}$ (and hence a mass of $10^9\,{\rm M}_\odot$). In conclusion, both massive evolved objects and/or strong starbursts may contribute to the counts at $z \geq 1.6$ and $K \leq 21$. As both classes are relatively rare in 'bottom-up' hierarchical models, the redshift distribution is a sensitive test for these models.

The agreement between the observed and predicted distribution is slightly worse at $z \leq 0.5$. The observed *differential* distribution (Fig.1c) has indeed a paucity of galaxies at very low redshifts with respect to the theoretical predictions, an effect that produces the steeper cumulative distribution shown in Fig.1(b). This is likely a combination of selection effects (these small fields have been explicitly chosen to be free of bright local galaxies) and the slope of the faint end of the luminosity functions in CDM models, which is steeper than locally observed.

4 THE COSMOLOGICAL EVOLUTION OF THE UV LUMINOSITY DENSITY

We show in Fig. 2 the cosmological evolution of the UV luminosity density ϕ_{2700} as estimated from the photometric redshifts at $I_{AB} \leq 26$ (HDF–N + HDF–S + NTTDF, left panels) and at $I_{AB} \leq 27.5$ (HDF–N + HDF–S, right panels), for two different cosmologies. The L_{2700} luminosity of each galaxy in the sample is directly obtained from the best-fitting spectrum, and

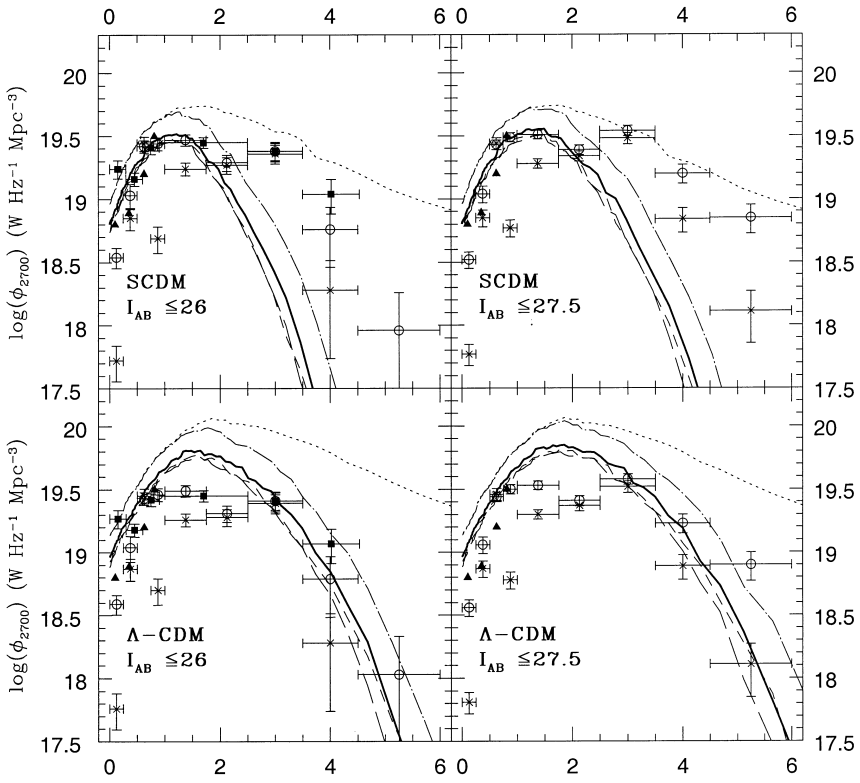

Figure 2. A comparison between the observed evolution of the luminosity density ϕ_{2700} and the predictions of hierarchical models. Empty circles are derived from the HDF–N, crosses from the HDF–S and filled squares from the NTTDF. Points are *not* corrected for incompleteness. Error bars are computed from the number of objects in the bins, assuming simple Poisson statistics. Triangles are taken from the spectroscopic surveys of Treyer et al. (1998) (lowest bin) and Lilly et al. (1995). From left to right, two different magnitude limits have been adopted, as shown in the figures. Upper panels are for standard CDM, lower panels for a Λ-dominated Universe. Theoretical curves are computed with our analytical rendition of hierarchical models for the relevant cosmology. The dotted line is the total UV luminosity density computed from the models assuming no dust absorption; the dot–dashed line is the same quantity when a magnitude cut corresponding to the magnitude limit in the data is applied; the thick solid line is for a magnitude cut + dust absorption (Calzetti); the short-dashed line for a magnitude cut + dust absorption (SMC); the long-dashed line for a magnitude cut + dust absorption (MW).

falls in the range of the observed magnitudes at any redshift $z > 0.25$. At $z > 2.4$, most objects are undetected in the IR bands, and the fitting spectra are constrained by the corresponding upper limits.

The availability of these three different fields allows us for the first time to compare the evolution of ϕ_{2700} in different fields. At $I_{AB} \leq 26$, the NTTDF is in good agreement with the HDF–N, while the HDF–S shows significant differences at $0.75 < z < 1.5$ and at $z > 3.5$, because of the variance in the total counts and the redshift distributions. At this stage, it is not clear whether the overall discrepancy among the fields, and most notably between HDF–N and HDF–S, is caused by real cosmic variance or some instrumental effect, and we consider it as an estimate of the global uncertainities in this analysis. At $z \leq 1.5$, the results from the NTTDF and the HDF–N are consistent with those from spectroscopic surveys (Treyer et al. 1998; Lilly et al. 1995) when the corrections for steep luminosity functions are adopted, as seems appropriate for fields dominated by blue star-forming galaxies. At higher z, all the fields concur with a scenario in which the UV luminosity density is relatively constant from $z = 1$ to $z = 4.5$.

The overall picture emerging from Fig. 2 is that the UV luminosity density does not change by more than a factor of 4 over the redshift range $0 < z < 4.5$, the only exception being the $z \simeq 4$ redshift bin in the HDF–S (but see below).

The comparison with CDM models is less straightforward here. We have overplotted in Fig. 2 the predictions of two well-studied examples, SCDM and ΛCDM. At variance with previous works, we have not corrected the observed values for incompleteness or extinction, but rather we have explicitly shown the differential effects of the inclusion of a magnitude limit and different dust extinction curves on the theoretical expectations. The comparison shows that the ϕ_{2700} overall shape is poorly fitted by the current CDM models. In particular, the SCDM model is not able to produce the density of UV photons that is observed at $z \geq 3$, while ΛCDM is in better agreement at $3 \leq z \leq 4.5$, but predicts a pronounced peak at $z \simeq 1.5$ and a drop by a factor of 8 from $z = 1.5$ to $z = 4$ that is not observed in the data.

A more accurate comparison at high redshift can be carried out by plotting (Fig. 3) the redshift evolution of the UV luminosity density at a shorter wavelength (1400 Å), where the best-fitting spectra are tied to the observed *R* and *I* bands, and compare it with spectroscopic surveys and CDM models. Photometric surveys are consistent with the results of spectroscopic surveys on brighter samples, with the exception of the HDF–S, especially at $z \geq 3.5$. The large variance between the HDF–N and the HDF–S is caused by an intrinsic lack of high-redshift galaxies in the latter. In particular, four objects are identified at $z \geq 5$ in the HDF–N, while no convincing candidate is found in the HDF–S, after removing obvious stars. It should be noted that when a standard colour selection as in Madau et al. (1996) is applied, a comparable number of *B*-dropout galaxies can be found in the HDF–N and S. However, these represent only a fraction of the high-redshift

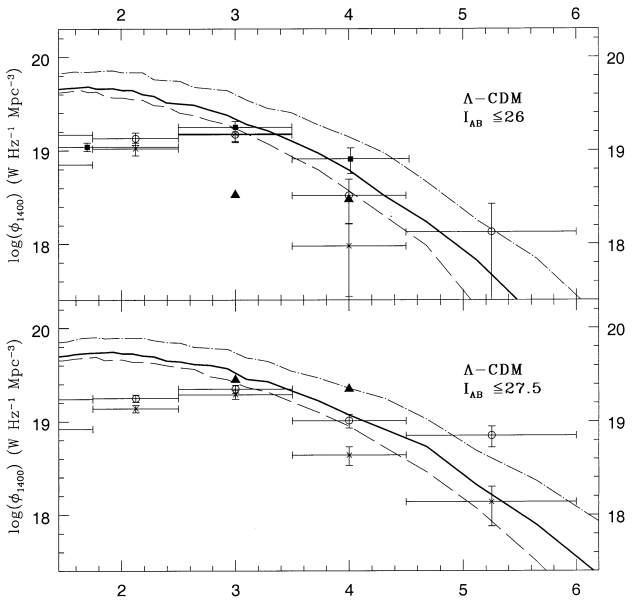

Figure 3. A comparison between the observed evolution of the luminosity density ϕ_{1400} and the prediction of hierarchical models. Triangles in the upper panel are from the spectroscopic data of Steidel et al. (1999). These have been corrected for incompleteness up to $I_{AB} = 27.5$ in the lower panel. All the other symbols and lines as in Fig. 2.

galaxies found by the photometric redshift technique (see Pascarelle, Lanzetta & Fernandez-Soto 1998; Fontana et al., in preparation), which uses the IR bands as additional constraints. These additional high-redshift candidates are brighter and more numerous in the HDF–N than in the HDF–S, producing the different values shown in Fig. 3.

5 SUMMARY

We have collected and analysed a sample of 1712 *I*-selected and 319 $K \leq 21$ galaxies from public deep imaging surveys, mainly from the two HDFs and the NTTDF. We have derived photometric redshifts for the whole sample in a homogeneous way. The results may be summarized as follows.

(i) The redshift distribution of the $K \leq 21$ sample (Fig. 1) is dominated by objects at low or intermediate redshift, with a fraction of only 9 per cent of galaxies detected at $z \geq 1.6$ and only 5 per cent at $z \geq 2$.

(ii) The UV luminosity density ϕ_{2700} grows by less than a factor of 4 from $z = 0$ to $z = 1$ (Fig. 2), and is relatively constant from $z = 1$ to $z = 4.5$, although significant field-to-field variations exist, and these dominate over statistical uncertainties.

(iii) A comparison between HDF–N and HDF–S shows that the UV luminosity density ϕ_{1400} at $z \geq 4.5$ is still poorly determined, probably because of the cosmic variance between these two small fields. ϕ_{1400} changes by a factor of 6 between the two fields at $z \geq 4.5$, because no convincing $z \geq 5$ candidate is found in the HDF–S, compared with four in the HDF–N (two of which have spectroscopic confirmation).

We have compared these results with the predictions of our analytical rendition of popular CDM models. We chose not to correct the data for incompleteness or dust extinction, but instead to include both effects in the theoretical model with which the comparison is made.

The $K \leq 21$ redshift distribution at $z \geq 1$ directly reflects the number of massive galaxies already assembled at $z \geq 1$ (KC98). The agreement that we find between the observed distribution and the prediction of an ensemble of CDM models (Fig.1b) strongly supports a key feature of these theoretical scenarios, i.e. the suggestion that massive objects are the result of merging processes in recent epochs.

On the other hand, the overall shape of the UV luminosity density, which is tied to the physical mechanisms driving the star formation processes, is not easily reproduced by current CDM models. The comparison between the observed evolution and the prediction of two different models (SCDM and ΛCDM) shows that the SCDM model is not able to produce the density of UV photons that is observed at $z \geq 3$. Given the $I_{AB} \leq 27.5$ limit applied to both observations and models, the discrepancy means that the current SCDM model fails to reproduce the bright tail of the luminosity function.

ΛCDM is in better agreement at $3 \leq z \leq 4.5$, but predicts a pronounced peak at $z \simeq 1.5$ and a drop by a factor of 8 from $z = 1.5$ to $z = 4$ that is not observed in the data. Such a result holds for all the adopted extinction laws. This implies that further refinements are required in the treatment of the physical processes directly related to the SFR. For instance, adopting a weaker feedback would increase the luminosity of fainter galaxies, which dominate the statistics at $z \geq 2$, yielding a less steep decline of the SFR. Another possibility is that merging activity at $z \geq 2$ is effective in enhancing the luminosity and/or the number density of faint galaxies at such *z*. A first attempt to include these effects has been described by Somerville, Primack & Faber (1998). These – or other – changes will require a global recalibration of the model parameters, in order to fit the increasing number of observables at low and high redshift.

ACKNOWLEDGMENTS

We thank Alvio Renzini for stimulating discussions on this research topics, the referee, Guinevere Kauffmann, for several useful comments which improved the paper and F. Governato, S. Savaglio and V. Testa for comments on earlier versions of this work.

This paper was based on observations made with the ESO VLT Antu telescope at the Paranal Observatory, the ESO New Technology Telescope at the La Silla Observatory [some of which were under the EIS programs 59.A-9005(A), 60.A-9005(A)], the NASA/ESA *Hubble Space Telescope* and the Kitt Peak National Observatory. The ultraviolet observations of the NTTDF were performed in SUSI-2 guaranteed time of the Observatory of Rome in the framework of the ESO-Rome Observatory agreement for this instrument.

REFERENCES

Arnouts S., D'Odorico S., Cristiani S., Zaggia S., Fontana A., Giallongo E., 1999a, A&A, 341, 641

Arnouts S., Cristiani S., Moscardini L., Matarrese S., Lucchin F., Fontana A., Giallongo E., 1999b, MNRAS, in press (astro-ph/9902290)

Baugh C. M., Cole S., Frenk C. S., Lacey C. G., 1998, ApJ, 498, 504

Bernardi M., Renzini A., da Costa L. N., Wegner G., Alonso M. V., Pellegrini P. S., Rité C., Willmer C. N. A., 1999, ApJ, 508, 143

Cohen J. G., Blandford R., Hogg D. W., Pahre M. A., Shopbell P. L., 1999, ApJ, 512, 30

Cole S., Aragón-Salamanca A., Frenk C. S., Navarro J. F., Zepf S. E., 1994, MNRAS, 271, 781

Connolly A. J., Szalay A. S., Dickinson M., SubbaRao M. U., Brunner R. J., 1997, ApJ, 486, L11
Cowie L. L., Songaila A., Hu E. M., Cohen J. G., 1996, AJ, 112, 839
Cowie L. L., Songaila A., Barger A. J., 1999, AJ, in press (astro-ph/9904345)
Da Costa L. et al., 1998, A&A, submitted (astro-ph/9812105)
Fernandez-Soto A., Lanzetta K. M., Yahil A., 1999, ApJ, 513, 34
Fontana A., D'Odorico S., Fosbury R., Giallongo E., Hook I., Poli F., Renzini A., Viezzer R., 1999, A&A, 343, L19
Giallongo E., D'Odorico S., Fontana A., Cristiani S., Egami E., Hu E., McMahon R. G., 1998, AJ, 115, 2169 (G98)
Guiderdoni B., Rocca-Volmerange B., 1987, A&A, 186, 1
Heyl J. S., Cole S., Frenk C. S., Navarro J. F., 1995, MNRAS, 264, 755
Hughes D. H. et al., 1998, Nat, 394, 241
Kauffmann G., Charlot S., 1998, MNRAS, 297, L23 (KC98)
Kauffmann G., White S. D. M., Guiderdoni B., 1993, MNRAS, 264, 201
Lacey C., Cole S., 1993, MNRAS, 262, L627
Lilly S. J., Tresse L., Hammer F., Crampton D., Le Fèvre O., 1995, ApJ, 455, 108
Madau P., Ferguson H. C. L., Dickinson M., Giavalisco M., Steidel C. C., Fruchter A., 1996, MNRAS, 283, 1388
Madau P., Pozzetti L., Dickinson M., 1998, ApJ, 498, 106
Menci N., Cavaliere A., 1999, MNRAS, in press (astro-ph/9909259)
Pascarelle S. M., Lanzetta K. M., Fernandez-Soto A., 1998, ApJ, 508, L1
Pei Y. C., 1992, ApJ, 395, 130
Poli F., Giallongo E., Menci N., D'Odorico S., Fontana A., 1999, ApJ, in press
Saracco P., D'Odorico S., Moorwood A., Buzzoni A., Cuby J.-G., Lidman C., 1999, A&A, 349, 751
Schade D. et al., 1999, ApJ, in press (astro-ph/9906171),
Somerville R. S., Primack J. R., 1998, MNRAS, submitted (astro-ph/9802268)
Somerville R. S., Primack J. R., Faber S. M., 1998, MNRAS, submitted (astro-ph/9806228)
Steidel C. C. M., Adelberger K. L., Giavalisco M., Dickinson M., Pettini M., 1999, ApJ, 519, 1
Treyer M. A., Ellis R. S., Milliard B., Donas J., Bridges T. J., 1998, MNRAS, 300, 303
White S. D. M., Frenk C. S., 1991, ApJ, 379, 52

This paper has been typeset from a TEX/LATEX file prepared by the author.